LETTER • OPEN ACCESS

# Multiple shapes from a single nematic elastomer sheet activated via patterned illumination

To cite this article: A. Giudici *et al* 2022 *EPL* **140** 36003

A Letters Journal Exploring the Frontiers of Physics

November 2022

EPL, **140** (2022) 36003
doi: 10.1209/0295-5075/ac9e19

www.epljournal.org

# Multiple shapes from a single nematic elastomer sheet activated via patterned illumination

A. Giudici[1(a)], A. Clement[2], D. L. Duffy[1], M. Ravi Shankar[2] and J. S. Biggins[1]

[1] *Department of Engineering, University of Cambridge - Trumpington St., Cambridge CB21PZ, UK*
[2] *Department of Industrial Engineering, Swanson School of Engineering - University of Pittsburgh, PA 15261, USA*

received 6 August 2022; accepted in final form 27 October 2022
published online 16 November 2022

**Abstract** – Liquid crystal elastomers (LCEs) undergo a large uniaxial contraction upon thermal or optical stimulation. LCE sheets are often fabricated with a spatially patterned direction of contraction, which can sculpt the sheet into a Gauss-curved surface. Here, we instead consider LCE sheets subject to patterned stimulation intensity, leading to a control of contraction strength. We show such patterns may also sculpt a complex surface, but with the advantage that arbitrarily many surfaces may be achieved sequentially in the same sample, thus breaking the link between microstructure and shape. We first consider a monodomain LCE in which some regions are actuated and others are not. We discuss how to join actuated and unactuated regions compatibly, and use this design rule to generate patterns for cones, anti-cones, arrays of cones and a rolling bi-strip. We validate the patterns numerically via elastic shell simulations and demonstrate them experimentally via patterned photo-chemical actuation. Secondly, we consider an LCE disk with an azimuthal director profile actuated by a radially varying stimulus. We show, theoretically and numerically, how to design a stimulation profile to sculpt any surface of revolution. Such re-configurable actuation offers enticing possibilities for haptics, robotics and locomotion.



**Introduction.** – Differential patterns of active deformation underpin many exquisite shape changes in biological systems [1,2], from growth-driven embryonic gastrulation to the muscle-powered beating of a heart. Correspondingly, there is great interest in synthesising soft active materials capable of patterned spontaneous deformations, which promise advances in soft robots and deployable structures [3]. For example, a sheet of gel fabricated with a patterned cross-link density will undergo a pattern of isotropic dilation on swelling, allowing one to program the sheet to undergo a sophisticated conformal transformation [4–7]. Alternatively, one may use a liquid crystal elastomer [8], which is a rubbery material incorporating mesogenic rods that align into a nematic phase. Upon heating or photo-chemical activation the alignment is disrupted, reflecting the conventional nematic-isotropic transition, and the LCE contracts uni-axially along its director [9]. Furthermore, LCE sheets can be fabricated with a spatial pattern of alignment/contraction [10–12], which has been used to morph flat sheets into cones, faces and other complex surfaces [13–21].

A limitation of both approaches is that the pattern is prescribed during manufacturing and cannot be amended. A recent study addressed this challenge in gels by incorporating photo-switchable elements [22], which allowed the local swelling magnitude to be reprogrammed optically. Here, we consider, theoretically and numerically, how a single LCE sheet can undergo reprogrammable shape changes by controlling the magnitude of the local activation strength, allowing different shapes to be selected during each activation (fig. 1). We also demonstrate experimentally how this may be achieved by photo-chemically stimulating an LCE with patterned light.

A central theme in the mechanics and geometry of thin sheets is Gauss's *theorema egregium* which dictates that the Gauss curvature of a surface —computed as the product of the two principal curvatures $K = \frac{1}{R_1}\frac{1}{R_2}$— cannot be modified isometrically [23]. Since stretch is energetically prohibitive relative to bend, passive thin sheets may easily be formed into developable $K = 0$ surfaces like

(a) E-mail: ag2040@cam.ac.uk (corresponding author)

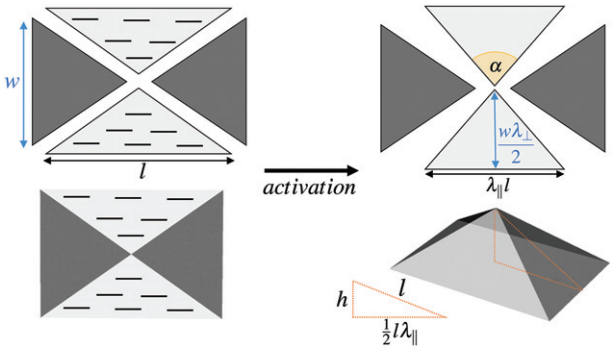


Fig. 1: Discrete pattern of deformation. The illuminated (bright) regions contract along the director and expand perpendicularly while the dark ones remain passive.

cylinders, but cannot be formed into Gauss-curved surfaces like spheres. In contrast, sheets that undergo a pattern of active shape change that varies in plane change their metric on activation, and can morph into Gauss-curved surfaces. Demonstrations of sheets that morph into surfaces with positive and negative $K$ have been the hallmark of flexible shape programming systems [4,22,24], and are the key building block for inverse design of surfaces with arbitrary Gauss-curvature distributions [13,19]. Furthermore, the *theorema egregium* guarantees that, once formed, such surfaces also may not be flattened without energetically prohibitive stretch. Correspondingly, LCE sheets that morph into cones bearing a point of singular positive $K$ at their tip, have proven to be capable of lifting thousands of times their own weight as they form [25].

To programme an arbitrary metric into an active sheet, one would need three independent actuation parameters at each point, reflecting the three components of a symmetric $2\times2$ matrix. However, in practice, most soft matter systems offer just one local degree of freedom: the magnitude of dilation in gels, and the direction of contraction in conventional LCEs. Patterning the stimulus magnitude in LCEs offers a distinct but rich palette as, although the liquid nematic-isotropic transition is first order, the contraction of LCEs is supercritical [9], with actuation occurring over a finite temperature window that may be narrow or broad depending on sample composition and preparation. An LCE fabricated with homogeneous director may thus be subject to a continuously patterned "grey-scale" stimulation to generate a variable contraction magnitude. This approach also leads to a metric with a single patternable degree of freedom —the local degree of contraction— which represents an interesting intermediate case between gels and conventional patterned LCEs.

Naturally, one may also consider an on/off pattern of stimulation, in which the contraction magnitude is a discrete patterning variable [26] dividing the sheet into contractile and passive regions. This approach is more limited, but offers a simpler stimulus control. Alternatively, one may superimpose patterned stimulation on a patterned director giving two degrees of freedom at each point [14], although only actuation strength is potentially reprogrammable. Here we consider two examples at the extremes of these possibilities: a monodomain subject to an on/off stimulation, and an LCE sheet with a circular director pattern subject to grey-scale stimulation.

**Discrete monodomain actuation.** – As our first example, we consider the actuation of a monodomain LCE sheet with director aligned along the horizontal $\hat{\boldsymbol{x}}$-direction. Homogeneous actuation simply leads to in-plane contraction of the sheet by a factor $\lambda_\parallel < 1$ along the director, and lateral elongation by a factor $\lambda_\perp \equiv \lambda_\parallel^{-\nu}$. LCEs are strictly volume conserving meaning $\nu = 1/2$. However, where possible we shall maintain the two components separate to encompass other anisotropic systems such as LC photo-glasses [27] ($\nu \sim 2$), and barromorphs ($\nu = 0$) [28].

Now, consider dividing the sheet into regions as shown in fig. 1, and activating only the regions shown in light grey. Free from constraints, the illuminated regions contract homogeneously, and the passive regions are unchanged. However, if we then try to recombine the pieces together, we find the puzzle is broken. The individual pieces are Gauss flat, but with the deformation there is now an angular deficit at the origin. The only solution to recombine them is to step out of the plane to create a surface with a singular point of positive Gauss curvature at the origin, for example by forming a rectangular pyramid.

However, our simple illustration in fig. 1 overlooks an important subtlety. We cannot arbitrarily choose boundaries between activated and non-activated regions, because the two regions may disagree on the length of their shared interface, leading to an ill-defined metric. Such incompatibility would result in material near the boundary being substantially stretched away from its preferred shape, inducing large (stretching) stresses, thickness-dependent deformations [29], wrinkling to accommodate excess length or, in brittle materials, perhaps even rupture. In contrast, the shapes that emerge from a sheet with a compatible metric are expected to be (bend-minimising) isometries, which are low stress and thickness independent. We thus ensure the two regions are geometrically compatible, mirroring the approach used in constructing piece-wise constant [30,31] and stitched [21,32] LCE director patterns.

To find such a compatible boundary, we must consider how distances change in the activated material as opposed to the passive one. Before actuation, a distance $\mathrm{d}l$ between any two points on the surface is given by the metric $\mathrm{d}l^2 = \mathrm{d}x^2 + \mathrm{d}y^2$. However, after activation, the length between the same points becomes $\mathrm{d}l_A^2 = \lambda_\parallel^2 \mathrm{d}x^2 + \lambda_\perp^2 \mathrm{d}y^2$. If the interface is parameterised by an arc-length parameter $s$ and makes an angle $\theta$ to the $x$-axis (fig. 2(a)) then $(\mathrm{d}x, \mathrm{d}y) = (\cos\theta, \sin\theta)\mathrm{d}s$. According to the activated region, the length of the interface is $\mathrm{d}l_A^2 = (\lambda_\parallel^2 \cos^2\theta + \lambda_\perp^2 \sin^2\theta)\mathrm{d}s^2$ while, for the non activated region, the local length of the boundary

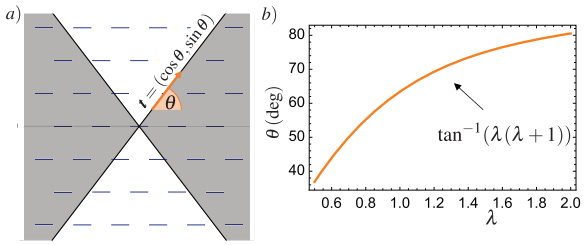


Fig. 2: (a) Sketch of the boundary line between two regions and its unit tangent vector $\boldsymbol{t} = (\cos\theta, \sin\theta)$. (b) Plot of $\theta$ as a function of $\lambda$, where $\lambda_\parallel = \lambda$ and $\lambda_\perp = 1/\sqrt{\lambda}$.

is simply $\mathrm{d}l = \mathrm{d}s$. For the two to agree, we must have $(\lambda_\parallel^2 \cos^2\theta + \lambda_\perp^2 \sin^2\theta) = 1$, which requires [32,33]

$$\theta = \pm \arctan(\gamma)\,, \tag{1}$$

where $\gamma = \sqrt{(1-\lambda_\parallel^2)/(\lambda_\perp^2 - 1)}$. Provided the two stretch ratios span unity, this result yields two compatible angles for the boundary line reflecting the up-down symmetry of the system. In the particular case of incompressible LCEs, the angle $\theta$ as a function of $\lambda_\parallel$ is shown in fig. 2(b). As the angle depends on the degree of actuation, a pattern designed for a target $\lambda_\parallel$ will not be compatible *en route*, unless the angle is adjusted during activation. However, even *en route*, the angle will typically only be wrong by a few degrees (fig. 2(b)) and largest when the strains are lower, so the degree of incompatibility is very mild.

In a planar monodomain, this angle is constant so the boundaries are straight lines. However, if the director varies in space, then so will the compatible angle, meaning the interface will be curved [32]. Alternatively, one may consider an LCE sheet with a homeotropic (normal) director, in which case both planar directions are orthogonal to the director, so activation gives the simpler actuation of isotropic dilation by $\lambda_\perp$. In this case, differential actuation generates a conformal metric, familiar from swelling gels [34]. Such a system is likely to be disappointing in practice, as it forgoes the most dramatic spontaneous strain, $\lambda_\parallel$. We now see that a second drawback of this approach is that the actuated length $\mathrm{d}l = \lambda_\perp \mathrm{d}s$ is strictly larger than $\mathrm{d}s$, so no compatible boundary exists [32] and compatible discrete actuation is not possible.

*Cones and anti-cones.* Returning to our planar monodomain, the compatible boundaries form straight lines in the reference state, so the previous design for a square pyramid is compatible provided the interfaces are angled appropriately. A simple geometric calculation reveals the height of the pyramid is $h = l\sqrt{(1-\lambda_\parallel^2)}$ and the angular deficit is $\Omega = 2(\arctan(\gamma^{-1}\frac{\lambda_\parallel}{\lambda_\perp}) - \arctan(\gamma^{-1}))$. Conversely, we may invert the pattern, actuating the horizontal wedges but not the vertical ones (fig. 3). The boundary remains compatible, but now the actuated regions expand vertically on activation, meaning their central angle increases. The sum of angles at the centre leads to an angular surplus $\Omega = 2(\arctan(\gamma\frac{\lambda_\perp}{\lambda_\parallel}) - \arctan(\gamma))$, generating to a saddle-like anti-conical surface with a singular point of negative Gauss curvature [24]. This confirms we can generate tips of positive and negative Gauss curvature.

We validate these designs numerically using a bespoke code, documented in [14], that minimizes an elastic energy (stretch + bend) for an active shell to predict its shape. As seen in fig. 3, the simulations confirm that the same sheet can attain surfaces with (anti-)tips of Gauss curvature at the origin after activation of the appropriate metric. Interestingly, the rectangular pyramid is not observed, as such a surface can relax isometrically to a conventional cone, thereby avoiding the singular bend associated with the folds. Similarly, the interfaces in the dual pattern are not visible in the actuated surface, which relaxes isometrically to a smooth anti-cone. In both cases the Gauss curvature in the simulated (anti-)tip is also not concentrated at a point but smeared out over a small but finite length-scale similar to the sheet thickness. This relaxation is also motivated by avoiding the singular bend of a sharp tip, but in this case there is no isometry available so relaxation incurs some localised stretch, as is familiar from conventional LCE cones [24].

To demonstrate our designs experimentally, we fabricated an azo-benzene doped LCE sheet with a longitudinal director orientation imprinted via mechanical stretching during cross-linking (see the Supplementary Material `Supplementarymaterial.pdf` (SM) for full details). To obtain the various shapes, the sheet was then constrained between glass slides and illuminated for 20 minutes with light intensity of 100 mW/cm$^2$ while using a mask to shadow the passive regions. The slides ensured the LCE remained in its flat reference configuration during activation, so that the desired regions could be activated straightforwardly. Illuminated regions became orange coloured, reflecting the isomerization in the azobenzene moieties into a bent *cis* state, which is known to disrupt the nematic order and generate a contraction [35]. During this constrained activation process, stresses build up in the sheet but, fortunately, the soft LCE can accommodate these without failure. After illumination the sheet is released, and relaxes to its final low-stress shape. Shape relaxation occurred over tens of seconds, and final steady-state photographs were taken 3 minutes after release. The resulting shapes were long-lived at room temperature (hours), so, to return to the original flat sheet before reprogramming, the system was let to rest overnight or illuminated with intense visible light for 2 minutes to stimulate azobenzene's back-reaction. Homogeneous illumination leads to a homogeneous activation strain of $\lambda_\parallel \sim 0.9$. Perhaps surprisingly, this modest strain was sufficient to generate convincing cone and and anti-cone surfaces, reflecting the fact that straight lines in a flat sheet are geodesics, so normal displacement and strain only couple at second order. Importantly, the resultant shapes (bottom row of fig. 3) were achieved sequentially in the same LCE sheet.

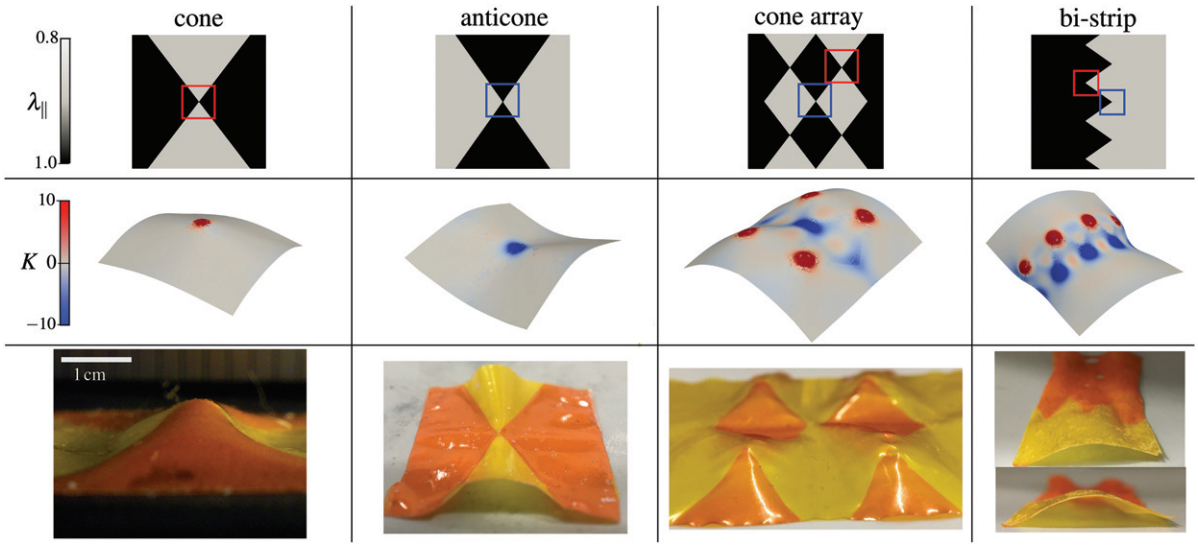


Fig. 3: Comparison of theoretical, numerical and experimental results for various patterns of discrete illumination. From left to right we have a cone, an anti-cone, an array of cones and a bi-strip. The simulations were run for LCEs with activation $\lambda_{\parallel} = 1/\sqrt{\lambda_{\perp}} = 0.8$, thickness to length ratio $t/l = 0.02$.

*Complex surfaces.* Many more shapes may be attained via different patterns of illumination. With discrete actuation, one may choose any pattern of active/passive separated by compatible interfaces, generating a design space that is comparably rich to the well-studied case of non-isometric origami [30,31]. Indeed, in both the current case and the non-isometric origami case, the individual regions are actuated homogeneously, so they always remain Gauss flat, as do the compatible interfaces between them. Therefore, such approaches generically produce surfaces with (anti-)tips of Gauss curvature stemming from vertices in the pattern and embedded in a Gauss flat landscape. This observation clarifies that cones and anti-cones are the natural building blocks for discrete actuation.

In the third column of fig. 3, we demonstrate a simple example of this concept by tessellating the original cone square pattern. The resulting metric contains an array of conical and anti-conical tips (circled in red and blue), and admits a tessellated array of pyramids as an exact isometry, reminiscent of the the LCE cone arrays that are such powerful lifters [25]. The pattern was also programmed in the same experimental LCE sheet to create an array with four conical tips, highlighting how a sheet can sustain shapes with different horizontal and vertical scales, potentially offering a route to switchable topography.

As a second example, we consider a sheet in which the right-hand side is active, and the left-hand side is passive (fig. 3, right column). If two regions are connected naively by a simple vertical line, it would be an incompatible boundary, and not admit any isometry. Such incompatible patterns were studied in [26] (using photo-thermal actuation patterned at fabrication via gold-nanoparticles), and were observed to produce a section of a bottleneck, in which the activated and passive region form sections of cylinders with different radii. The overall bottleneck shape accommodates both halves isometrically, except in the neck region (corresponding to the boundary) where bands of positive and negative $K$ highlight that material has had to distort. Here, we instead construct a compatible boundary by zig-zagging at the compatible angle, producing a compatible metric with the same overall character. The zig-zags then encode a ring of positive tips and a ring of negative tips, leading to a metric that would admit a faceted section of a bottleneck as an exact isometry, similar to the (non-isometric origami) example in [36]. As previously, simulation and experiment reveal that such facets are actually able to relax, leading to a final shape that is very similar to that seen in bi-strip in [26,29], though the discrete tips are visible in the numerically evaluated $K$.

**Shells of revolution via differential illumination.** – As our second example, we consider a more complex system with a continuous activation modulation superimposed on a patterned director. More precisely, we consider an LCE disk fabricated with a director pattern in concentric circles, and then subject to stimulation that can be prescribed as a continuous function of the (reference state) radial coordinate, $\lambda_{\parallel}(R)$, $\lambda_{\perp}(R) = \lambda_{\parallel}(R)^{-\nu}$. As shown in fig. 4, such stimulation will cause the disk to morph into a surface of revolution, generating a similar family of shapes as those generated by radially varying director angles in homogeneous actuation [37–39]. Our aim is to understand the relationship between the activation strength, and the resulting surface of revolution, in order to tackle the inverse problem of finding the actuation field $\lambda_{\parallel}(R)$ required to generate a given surface.

As shown in fig. 4, any surface of revolution may be described by $\psi(\rho)$, which gives the in-space cylindrical radius $\psi$ as a function of the in-shell radial arc-length $\rho$. The

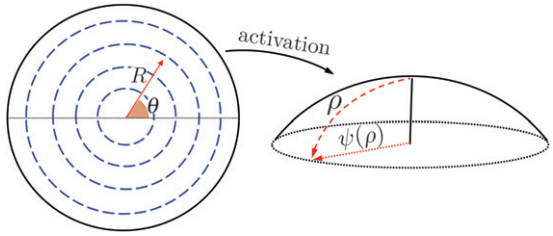


Fig. 4: On the left, a point with $R$, $\theta$ coordinates on a sheet decorated with azimuthal director field. On the right, the geometrical meaning of the $\rho$, $\psi$ coordinates, where the first represents the arclength distance and the second the distance of a point on the surface from the axis of revolution.

surface is then paramaterized by $(\rho, \theta)$ coordinates (where $\theta$ is the azimuthal angle) as

$$\boldsymbol{r}(\rho,\theta) = \left(\psi(\rho)\cos(\theta), \psi(\rho)\sin(\theta), \int_0^\rho \sqrt{1-\psi'(s)^2}\mathrm{d}s\right),$$

leading to the metric

$$\mathrm{d}l_A^2 = \mathrm{d}\rho^2 + \psi(\rho)^2\mathrm{d}\theta^2, \tag{2}$$

and the Gauss curvature distribution $K(\rho) = -\frac{\psi''(\rho)}{\psi(\rho)}$.

To connect this description of a surface of revolution to the LCE disk, we consider a circle on the sheet centred at the origin and with radius $R$. After actuation, the length of the circle shrinks by a factor of $\lambda_\parallel < 1$, requiring

$$\psi = \lambda_\parallel R. \tag{3}$$

In contrast, radial distances increase by $\lambda_\perp > 1$ on actuation, so that the arclength distance of the circle from the centre after actuation is

$$\rho = \int_0^R \lambda_\perp(R')\mathrm{d}R' = \int_0^R \lambda_\parallel^{-\nu}(R')\mathrm{d}R' > R. \tag{4}$$

Equations (3) and (4) give $\rho(R)$ and $\psi(R)$, effectively solving the forward problem of shape from pattern. To tackle the inverse problem, we combine these results to write

$$\frac{\mathrm{d}\rho}{\mathrm{d}R} = \lambda_\parallel^{-\nu} = \left(\frac{R}{\psi(\rho)}\right)^\nu. \tag{5}$$

This equation can be integrated leading to

$$R(\rho) = \left[(1+\nu)\left(\int_0^\rho \psi(\rho')^\nu \mathrm{d}\rho' + c\right)\right]^{1/(1+\nu)}, \tag{6}$$

where the constant of integration, $c$, must vanish in a closed disk, but would be permitted if the disk is pierced by a hole, in which case it controls the relationship between the initial and final radius of the hole itself. The above result allows us to construct, for any surface $\psi(\rho)$, the original reference radius $R$ for each actuated arclength $\rho$. The inverse problem is then solved by inserting this result into eq. (3), to give

$$\lambda_\parallel(\rho) = \psi(\rho)/R(\rho). \tag{7}$$

From $\lambda_\parallel/\rho)$, one may finally construct the desired function $\lambda_\parallel(R)$, by numerically inverting $R(\rho)$ and substituting, or by plotting $\lambda(\rho)$, parametrically against $R(\rho)$. We thus see that, for a closed disk, any surface may be targeted, and there is a unique pattern of actuation to achieve it. Of course one must check that the required $\lambda_\parallel$ is achievable by the sample.

**Examples: flat, positive and negative Gauss curvature surfaces.** – We illustrate the above result by presenting several examples of actuation profiles for LCE sheets with azimuthal director orientation and optothermal Poison ratio $\nu = \frac{1}{2}$. In this case, eq. (6) specialises to

$$R(\rho) = \left[\frac{3}{2}\left(\int_0^\rho \sqrt{\psi(\rho')}\mathrm{d}\rho' + c\right)\right]^{2/3}. \tag{8}$$

We consider two different initial sample shapes: a disk and an annulus, and discuss a variety of possible shape changes we can program on the same two samples.

*Disk.* We first consider that the LCE sheet is the unit disk. In this case, a uniform actuation leads simply to $\psi = \lambda_\parallel R$ and $\rho = \lambda_\perp R$, and hence the surface $\psi(\rho) = (\lambda_\parallel/\lambda_\perp)\rho$ which describes a cone with semi angle $\alpha = \arcsin(\lambda_\parallel/\lambda_\perp)$ at the tip [30]. This simple actuation profile, and the simulated shape of the cone are shown in fig. 5(a)(i).

Next, let us derive the function $\lambda_\parallel(R)$ necessary to create a surface of constant positive Gauss curvature: a spherical cap. In this case, we need $\psi(\rho) = A\sin(\rho/A)$ where $A$ is the radius of the sphere, meaning the Gaussian curvature is $K = \frac{1}{A^2}$. Equation (6) can then be integrated to obtain

$$R(\rho) = 3^{\frac{2}{3}} A\left(\frac{\Gamma\left(\frac{3}{4}\right)^2}{\sqrt{2\pi}} - E\left(\frac{1}{4}\left(\pi - \frac{2\rho}{A}\right)\middle|\, 2\right)\right)^{2/3}, \tag{9}$$

where $E(\phi|\, m) = \int_0^\phi \sqrt{1 - m\sin^2 u}\mathrm{d}u$ is the elliptic integral of the second kind, $\Gamma(x)$ is the Euler gamma function and we set $c = 0$ to ensure $R(0) = 0$. From (7), we find

$$\lambda_\parallel(\rho) = A\sin(\rho/A)/R(\rho). \tag{10}$$

The activation profile is plotted parametrically against $R$ in fig. 5(a)(ii), as is the resulting simulated final shape of the shell.

The cone and the spherical cap are two simple examples of constant Gauss curvature surfaces. In fig. 5(a)(iii) we show how a much more complex surface, with alternating regions of positive and negative Gauss curvatures, can be obtained using this framework. In the inset on the side of the simulation, we compare the profile of the desired shape with numerical results, with excellent agreement.

*Annulus.* Finally, we consider activating an LCE annulus, with unit outer radius, and inner radius $R_i = 0.5$. In this case, homogeneous actuation will simply lead to a truncated cone with the same semi-angle as the disk case. However, in the annular geometry the constant of integration $c$ is permitted and allows for more freedom when

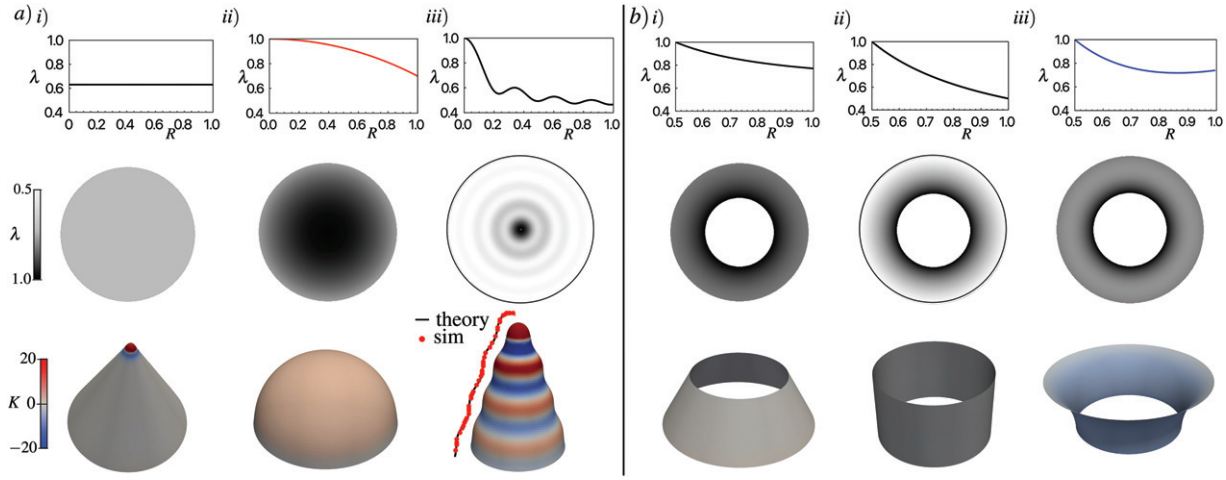


Fig. 5: Surfaces of revolution obtained modulating light intensity in an LCE sheet decorated with azimuthal director pattern. The top row shows the actuation function in the radial coordinate, the middle row shows images of the illumination strength and the bottom row shows numerical simulations of the LCE sheet using a 2D finite element code [14] for sheets of thickness to radius ratio 0.1. Panel (a) shows the shapes obtained from a disk of radius 1: (i) a cone of half angle $\sin\alpha = 0.5$, (ii) a spherical cap with radius of curvature $R = 0.7$, (iii) a complex surface alternating regions of positive and negative GC. Here, we compare the profile of the shape with red dots against the black theory line. (b) Surfaces obtained by an annulus of outer radius 1 and inner radius 0.5: (i) a truncated cone of half angle $\sin\alpha = 0.5$, (ii) a cylinder, and (iii) a catenary of revolution with $K = -2.8$. The inner radius of the annulus was kept constant during deformation.

choosing an actuation profile for a given surface. As explored in [40] for radially varying director patterns with homogeneous actuation, we may use $c$ to attain more dramatic surfaces, or to specify the actuated radius of the inner or outer boundary. For example, we may target a cone, but with the inner hole constrained to not change radius, requiring $\lambda_\parallel = 1$ on the inner boundary. To find the activation function, we write our target truncated cone as $\psi = R_i + \rho\sin\alpha$ with $\rho = 0$ on the boundary. Solving eq. (6) with $R(0) = R_i$ then leads to $c = \frac{2}{3}R_i^{3/2}$ and

$$R = ((\rho + \csc(\alpha)R_i)\sqrt{\psi} - ((\csc(\alpha) - 1)R_i^{3/2}))^{2/3},$$
$$\lambda = \psi((\rho + \csc(\alpha)R_i)\sqrt{\psi} - ((\csc(\alpha) - 1)R_i^{3/2}))^{-2/3}.$$

As expected, $\lambda_\parallel(R)$ is not constant, but increases as we move radially outwards, as shown in fig. 5(b)(i). Moreover, we are not limited to the original $\alpha$ in this expression, but may set it to any value to obtain cones of different steepness —illustrating that $c$ also enables more dramatic surfaces. Indeed, if we set $\alpha = \pi/2$, we can morph into a cylinder with

$$R = \psi(\sqrt{\psi}R_i + \rho\sqrt{\psi})^{-2/3}, \tag{11}$$
$$\lambda = \psi(\rho\sqrt{\psi} + R_i\sqrt{\psi})^{-2/3}. \tag{12}$$

As a final illustration, we can also obtain a negative Gauss-curved surface by letting $\psi(\rho) = R_i\cosh(\rho/A)$ so that $K = -\frac{1}{A^2}$. We note that this solution is only valid for $A < \rho/\sinh^{-1}(R_i)$ since otherwise $\sqrt{1-\psi'(\rho)^2}$ yields a complex solution, indicating the surface is not well defined. If we again fix $R(0) = R_i$ by setting $c = \frac{2}{3}R_i^{3/2}$ and using the complex number $i$ for conciseness, eq. (6) leads to

$$R(\rho) = R_i^{1/3}\left(R_i - 3iA/, E\left(i\rho/2A \,|\, 2\right)\right)^{2/3}, \tag{13}$$
$$\lambda(\rho) = A\cosh(\rho/A)/R(\rho). \tag{14}$$

This is a real function, plotted in fig. 5(b)(iii).

**Conclusion.** – We have considered how an LCE sheet can morph into a Gauss-curved surface via a spatial pattern of actuation strength, rather than the classic pattern of director orientation. Our study encompasses both discrete and continuous patterns of activation as well as sheets patterned with homogeneous and concentric director fields. Moreover, we have demonstrated how the actuation strength can be controlled using light intensity in LCEs, offering a simple route to sequential shapes.

In our experiments, the LCE was constrained to remain in the flat reference state during illumination, and was only released to attain its final shape afterwards. An important future direction is to instead impose a pattern of light on an unconstrained sample, that morphs as it is illuminated. In this case, the light intensity pattern would have to be adapted to account for the movement of material, and also the dilution of flux when the surface attains a finite gradient. In such circumstances, implementing a dynamic feedback system between light pattern and shape, may allow the system to hone in on the desired target.

The reconfigurable morphing of LCE sheets points to applications in robotics and haptics, although slow material response remains a key barrier (see the SM). Even with limited reconfigurability, the ability to generate non-reciprocating cycles of shape allows for swimming or pumping at low Reynolds number, and may be useful

for cyclic machines. Moreover, the ability to elicit shape multiplicity from a single monolith allows for the design of soft robots with nearly flat form factors. Motility on arbitrary surfaces (solid or fluid) can be modulated without predefined one-to-one mapping between micro-structure and actuated shape. Finally, solving the inverse problem would allow an LCE sheet to become a haptic display, generating any texture.

* * *

JSB acknowledges the UKRI Future Leaders Fellowship program, grant number MR/S017186/1. DLD is supported by the EPSRC Centre for Doctoral Training in Computational Methods for Materials Science, grant No. EP/L015552/1. MRS acknowledges support from the National Science Foundation (No. 1921842).

*Data availability statement*: All data that support the findings of this study are included within the article (and any supplementary files).

REFERENCES

[1] Thompson D. W., *On Growth and Form*, Vol. **2** (Cambridge University Press) 1942.
[2] Goriely A., *The Mathematics and Mechanics of Biological Growth*, Vol. **45** (Springer) 2017.
[3] El-Atab N., Mishra R. B., Al-Modaf F., Joharji L., Alsharif A. A., Alamoudi H., Diaz M., Qaiser N. and Hussain M. M., *Adv. Intell. Syst.*, **2** (2020) 2000128.
[4] Sharon E. and Efrati E., *Soft Matter*, **6** (2010) 5693.
[5] Kim J., Hanna J. A., Byun M., Santangelo C. D. and Hayward R. C., *Science*, **335** (2012) 1201.
[6] Na J.-H., Bende N. P., Bae J., Santangelo C. D. and Hayward R. C., *Soft Matter*, **12** (2016) 4985.
[7] Gladman A. S., Matsumoto E. A., Nuzzo R. G., Mahadevan L. and Lewis J. A., *Nat. Mater.*, **15** (2016) 413.
[8] Warner M. and Terentjev E. M., *Liquid Crystal Elastomers*, Vol. **120** (Oxford University Press) 2007.
[9] Küpfer J. and Finkelmann H., *Makromol. Chem., Rapid Commun.*, **12** (1991) 717.
[10] de Haan L. T., Sánchez-Somolinos C., Bastiaansen C. M., Schenning A. P. and Broer D. J., *Angew. Chem., Int. Ed.*, **51** (2012) 12469.
[11] Ware T. H., McConney M. E., Wie J. J., Tondiglia V. P. and White T. J., *Science*, **347** (2015) 982.
[12] Ambulo C. P., Burroughs J. J., Boothby J. M., Kim H., Shankar M. R. and Ware T. H., *ACS Appl. Mater. Interfaces*, **9** (2017) 37332.
[13] Aharoni H., Xia Y., Zhang X., Kamien R. D. and Yang S., *Proc. Nat. Acad. Sci. U.S.A.*, **115** (2018) 7206.
[14] Duffy D. and Biggins J. S., *Soft Matter*, **16** (2020) 10935.
[15] Warner M., *Annu. Rev. Condens. Matter Phys.*, **11** (2019).
[16] Warner M. and Mostajeran C., *Proc. R. Soc. A: Math., Phys. Eng. Sci.*, **474** (2018) 20170566.
[17] Mostajeran C., *Phys. Rev. E*, **91** (2015) 062405.
[18] Mostajeran C., Warner M., Ware T. H. and White T. J., *Proc. R. Soc. A: Math., Phys. Eng. Sci.*, **472** (2016).
[19] Griniasty I., Aharoni H. and Efrati E., *Phys. Rev. Lett.*, **123** (2019) 127801 (`http://arxiv.org/abs/1902.09902`).
[20] Feng F., Biggins J. S. and Warner M., *Phys. Rev. E*, **102** (2020) 13003.
[21] Duffy D., Cmok L., Biggins J., Krishna A., Modes C. D., Abdelrahman M., Javed M., Ware T., Feng F. and Warner M., *J. Appl. Phys.*, **129** (2021) 224701.
[22] Kuenstler A. S., Lahikainen M., Zhou H., Xu W., Priimagi A. and Hayward R. C., *ACS Macro Lett.*, **9** (2020) 1172.
[23] Kühnel W., *Differential Geometry*, Vol. **77** (American Mathematical Society) 2015.
[24] Modes C., Bhattacharya K. and Warner M., *Proc. R. Soc. A: Math., Phys. Eng. Sci.*, **467** (2011) 1121.
[25] Guin T., Settle M. J., Kowalski B. A., Auguste A. D., Beblo R. V., Reich G. W. and White T. J., *Nat. Commun.*, **9** (2018) 1.
[26] Kuenstler A. S., Chen Y., Bui P., Kim H., DeSimone A., Jin L. and Hayward R. C., *Adv. Mater.*, **32** (2020) 2000609.
[27] Liu D. and Broer D. J., *Nat. Commun.*, **6** (2015) 1.
[28] Siéfert E., Reyssat E., Bico J. and Roman B., *Nat. Mater.*, **18** (2019) 24.
[29] Kim J., Hanna J. A., Hayward R. C. and Santangelo C. D., *Soft Matter*, **8** (2012) 2375.
[30] Modes C. D. and Warner M., *Phys. Rev. E*, **84** (2011) 021711.
[31] Plucinsky P., Lemm M. and Bhattacharya K., *Phys. Rev. E*, **94** (2016) 010701.
[32] Feng F., Duffy D., Warner M. and Biggins J. S., *Proc. R. Soc. A.: Math. Phys. Eng. Sci.*, **478** (2022) 20220230.
[33] Huang Y., Biggins J., Ji Y. and Terentjev E., *J. Appl. Phys.*, **107** (2010) 083515.
[34] Klein Y., Efrati E. and Sharon E., *Science*, **315** (2007) 1116.
[35] Finkelmann H., Nishikawa E., Pereira G. and Warner M., *Phys. Rev. Lett.*, **87** (2001) 015501.
[36] Modes C. D. and Warner M., *The activated morphology of grain boundaries in nematic solid sheets*, in *Emerging Liquid Crystal Technologies VII*, *Proceedings of SPIE*, Vol. **8279** (SPIE) 2012, pp. 127–134.
[37] Mostajeran C., Warner M., Ware T. H. and White T. J., *Proc. R. Soc. A: Math. Phys. Eng. Sci.*, **472** (2016) 20160112.
[38] Kowalski B. A., Mostajeran C., Godman N. P., Warner M. and White T. J., *Phys. Rev. E*, **97** (2018) 012504.
[39] Warner M. and Mostajeran C., *Proc. R. Soc. A: Math. Phys. Eng. Sci.*, **474** (2018) 20170566.
[40] Duffy D., Javed M., Abdelrahman M., Ware T., Warner M. and Biggins J., *Phys. Rev. E*, **104** (2021) 065004.